Results in Engineering 24 (2024) 103274

Contents lists available at ScienceDirect

Results in Engineering

journal homepage: www.sciencedirect.com/journal/results-in-engineering

Research paper

Investigating enhanced electrical conductivity for antenna applications through dual metallization on 3D printed SLA substrates

Ahmad Nurhelmy Adam [a], Irfan Yahaya [a], Ahmad Adnan Abu Bakar [a], Shahino Mah Abdullah [a], Nizam Tamchek [b], Ahmad F. Alforidi [c], Ahmed Alahmadi [c], Mohd Haizal Jamaluddin [d], Mohd Azraie Mohd Azmi [e], Mohd Ifwat Mohd Ghazali [a,f,*]

[a] *SMART RG, Faculty of Science and Technology, Universiti Sains Islam Malaysia, Bandar Baru Nilai, Nilai 71800, Negeri Sembilan, Malaysia*
[b] *Department of Physics, Faculty of Science, Universiti Putra Malaysia, Serdang 43400, Selangor Darul Ehsan, Malaysia*
[c] *Department of Electrical Engineering, Taibah University, P.O. Box 344, Al-Madina Al Munawara 42353, Saudi Arabia*
[d] *Wireless Communication Centre, Universiti Teknologi Malaysia, Johor Bahru, 81310, Malaysia*
[e] *British-Malaysia Institute (BMI), Universiti Kuala Lumpur, Gombak, Selangor, 53100, Malaysia*
[f] *Department of Engineering, University of Cambridge, Trumpington Street, Cambridge, CB2 1PZ, United Kingdom*

A R T I C L E I N F O

Keywords:
Additive Manufacturing
patch antenna
3D printing
stereolithography (SLA)
simulated
metallization
Vector Network Analyzer (VNA)

A B S T R A C T

The advancement of 3D printing (additive manufacturing) has gained interest in variety of applications, especially for antenna fabrication. The demand for cheap, reliable, and high-performance antenna fabrication methods is essential in order to cope with the demand of wireless communications industry. In this work, the focus was emphasized on enhancing the electrical conductivity of the 3D printed substrates fabricated by stereolithography (SLA) 3D printer. The 3D printed substrate went through a dual metallization approach, involving sputtering and electrodeposition techniques for the fabrication of conductive metal layers. The parameters for the sputtering were fixed for all the substrate while current density during electrodeposition process was varied at 25 %, 50 %, 75 % and 100 % from recommended value of current. The results showed that the current density during the electrodeposition determined the conductivity performance of the metal layers and established a significant correlation with the surface morphological. Three different frequencies comprised of 2.4 GHz, 3.5 GHz and 5.0 GHz were selected to simulate and fabricate a microstrip patch antenna using the optimized current density which was valued optimal at 75 % (52.5 mA). The percentage of accuracy between simulated and measured frequencies of antenna, portrayed that the measured values were slightly higher than the simulated approximately about 5.14 to 6.67 %. Therefore, the integration of additive manufacturing or 3D printing techniques for antenna could address the critical necessity for fast and economical solution in wireless systems.

1. Introduction

Additive manufacturing or also known as 3D printing technology has emerged as a key feature for the Forth Industrial Revolution (IR 4.0), playing a vital role in shaping the landscape for future manufacturing [1–3]. The technology emphasizes forming three-dimensional (3D) structure through additive processing where materials are layered on top of one another in a sequential manner based on digital information typically according computer-aided design (CAD) file [4]. Technology has evolved from fabricating prototypes to manufacturing final products for a plethora of applications which includes automotive, aerospace, medical, dental, construction, robotics, education, and fashion [5,6]. Unlike its predecessor, subtractive manufacturing usually fabricates an object by removing materials such as solid blocks of rods, plastic, or metal to create a desired design. Thus, it produces high materials wastage and could become a hidden cost towards manufacturer [7]. Therefore, 3D printing could tackle this issue since the materials waste can be negligible. Nevertheless, other distinct features have captured the interest of specific industries, namely the electronics industry, prompting the usage of these technologies to develop alternative manufacturing for electronic devices in particular antenna application.

An antenna is a device that specialized in converting electric currents into electromagnetic waves (EM) or vice versa allowing radio-frequency communication between distant locations [8]. Antennas are used to

* Corresponding author.
E-mail address: ifwat.ghazali@usim.edu.my (M.I.M. Ghazali).

https://doi.org/10.1016/j.rineng.2024.103274
Received 17 July 2024; Received in revised form 26 September 2024; Accepted 28 October 2024
Available online 30 October 2024

either to transmit or receive non-ionizing EM field which include radio waves, microwaves, infrared radiation (IR) and visible light [9,10]. The first two formers are extensively used by the industries and public. They are typically classified as either transmitter or receiver, but can also act as dual function know as transceiver [11]. They are being classified by their design for instance aperture, array, reflector, lens, wire and microstrip antenna [12–16]. Each of these designs are established to operate for a specific application. Among them, microstrip antennas are widely known used in various wireless applications for instance wireless communications, satellite communications, radar systems, remote sensing and medical devices [17–21]. These could be attributed from their compact size, ease of fabrication, versatile and cost effectiveness for mass production [22].

Conventionally, the antenna fabrication process starts with the selection of the dielectric substrate which has pre- determined parameters by the manufacturer, followed by the deposition of conductive metal layer on the substrate, usually copper based metal. A process called photolithography is used to pattern an antenna geometrical design, in which subsequently will be etching during the chemical process to obtain desired design of antenna [23]. This process involves multi-stage levels along with intricate procedures, demanding specialized equipment and expose towards hazardous chemicals [24]. Other drawbacks are the limitation in terms of complex and precise structure of antenna design, limited for substrate material compatibility due to the deposition of metal, risk of human error and the labor-intensive nature of the process which demand constant supervision. The application of 3D printing technology as a manufacturing tool in antenna fabrication can effectively tackle these issues. In recent years the utilization of 3D printing technology has emerged as an alternative fabrication method for antenna fabrication [25,26]. Notably, 3D printers such as fused deposition modelling FDM, inkjet 3D printers and stereolithography (SLA) printers are capable in designing 3D printing antenna.

FDM is considered as a predominant 3D printing technology utilized not only for general 3D structure but also fabrication of complex antenna design. The 3D inkjet printing has gained recognition in antenna fabrication due to several advantages in possesses including high-resolution, able to print on conform surface, and able to print on a variety of materials [27]. The versatility of the 3D inkjet printing has demonstrated a variety of unique antenna designs which includes Yagi-uda, helical, RFID, dipole, slot antenna, horn antenna, dipole antenna and even dielectric resonator antenna [28,29]. Conversely, the drawback to FDM is the limited resolution at lateral axis printing direction (approximately $\pm$0.8 mm) and produce a very rough finish surface quality [30]. This restraint its capability to design for high frequency that could contribute towards signal losses due to the uneven surface roughness [31,32].

Meanwhile, 3D inkjet printing come across a problem related towards the conductivity of printed materials. The conductive ink for 3D inkjet printers typically exhibited lower conductivity compared to traditional metallic materials commonly used in antennas [33]. This could result in increased signal losses and reduced overall antenna efficiency. Additionally, the layer-by-layer deposition process inherent in 3D printing can introduce discontinuities in the antenna structure, leading to impedance mismatches and unwanted scattering effects [34, 35].

Among these 3D printing techniques, strereolithography (SLA) is considered as one of the most promising methods for printing antenna. SLA has a unique printing process where liquid resin will interact with UV light which then polymerizes the resin to form a 3D structure [36]. These capabilities allow the printing structure to be more accurate and able to do complex structure which is suitable for antenna fabrication [22]. However, one of the limitations for SLA technology to fabricate the antenna is due to the metallization of the 3D printed structure. Several efforts have been made by using electrodeposition and sputtering technique to metalize the 3D printed substrate. However, delamination of printed layers occurred due to weak adhesion between the metal layer and SLA printed structure.

This research was conducted to evaluate the influence of dual metallization consists of sputtering and electrodeposition on 3D printed SLA substrates towards electrical conductivity performance of microstrip patch antenna. The initial step involved sputtering the 3D printed SLA substrates with two different metals which were titanium and copper. These layers served as precedent layers for subsequent electrodeposition process. The electrodeposition process demands subjecting the 3D printed SLA substrate to vary current densities for monitoring copper layer formation that became a key determinant of metallization conductivity. The optimization of current density for electrodeposition of copper layer was evaluated by analyzing the correlation between the electrical conductivity and surface morphological of surface metal layers.

The optimized value of current density for electrodeposition process was subsequently employed in the fabrication of 3D printed substrates for microstrip patch antennas that operated across different frequencies: 2.4 GHz, 3.5 GHz, and 5.0 GHz. This frequency variation was crucial for evaluating the metal layer's ability across numerous wireless communication circumstances. The insights of this research provide an ample understanding and exploring the potential of 3D printing in the fabrication of substrate using SLA technique for antenna fabrication. The simplicity and customization of 3D printing have broaden the limitation of fabrication process for diverse wireless communications field. Fig. 1 shows the illustration of antenna applications that existed around us.

2. Materials and methods

2.1. Sample preparation

A sample substrate with screw holes was designed in computer-aided design (CAD) software to enable different preparation process and testing method with consistent sample as shown in Fig. 2. A circle substrate was designed with a 4.3 cm radius and 1.6 mm thickness. The design was printed using stereolithography (SLA) 3D printer (Form 2, Formlabs, Somerville, MA, USA) with ultraviolet (UV) curable high temperature resin from Formlabs. The 3D printer is equipped with 405 nm laser with optical power of 250mW. Printed samples were subjected to post process involving cleaning with isopropanol (IPA) and cured using UV cure machine (Formcure, Formlabs, Somerville, MA, USA) for 60 min.

2.2. Metallization process

The sample undergone metallization process to add conductive layers by deposition a blanket seed layer of titanium and copper by using DC sputtering system by Kurt J. Lesker (PRO Line PVD 75, Jefferson

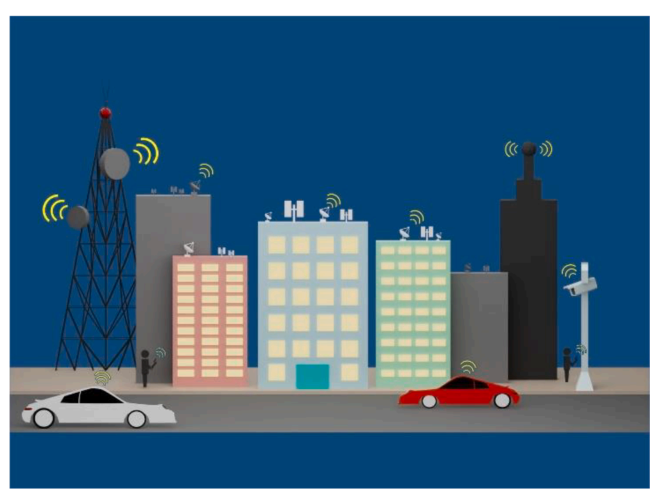

Fig. 1. Overall view application of wireless communication.

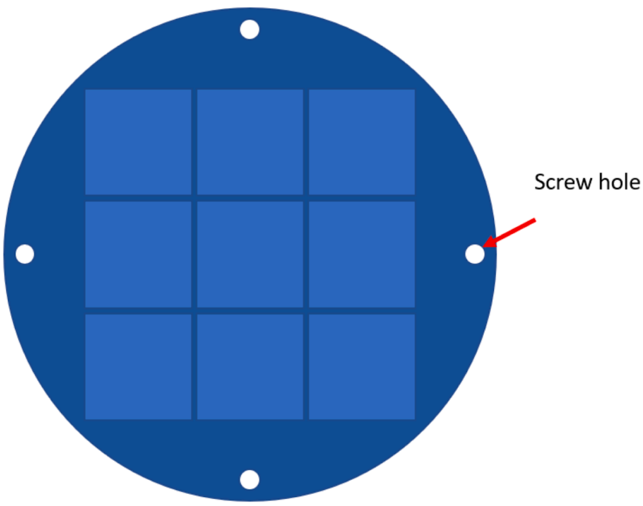

Fig. 2. Schematic drawing of the sample design.

Hills, PA, USA) [37]. A blanket layer of titanium was used to improve the adhesion between 3D printed sample and the copper layer [22,38]. The process parameters for metal deposition were shown in the Table 1.

The 3D printed substrate was then proceeded to another process of adding an additional layer of copper by using the electrodeposition technique. The process was used to provide the required conductor thickness for the radio-frequency (RF) applications and to improve the surface uniformity of the substrate. By running an electrical current through a solution containing copper ions, copper was electroplated onto a substrate, such as metal or plastic, to form a thin film of copper metal. Electrodeposition set-up of Caswell Inc's Plug N' Plate® Acid Copper Kit was used in this experiment. Samples were connected to cathode terminal while a copper sheet (electrode) was connected to anode terminal, whereas the copper sulfate was used as the solution. Before electrodeposition process started, the substrate would undergo surface treatment using sulfuric acid. The thickness of the copper layer can be controlled by adjusting the voltage, current density, and duration of electrodeposition process. The current density of the electrodeposition process was varied from the recommended value of current which was 70 mA per square inch provided by Caswell Inc. The electrodeposition process was done with different current densities as shown in Table 2 below for 30 min to study the effect of surface uniformity on the conductive paths. After the process, the samples were then taken out and washed with deionized water to get rid of any surplus solution. The samples were promptly cloth-dried and put inside an oven at 60 °C for drying. All samples have been coated with titanium for 35 min, copper for 30 min, and different current density for copper electrodeposition (%). Table 3 shows the sample name according to the current density for copper plating (%).

2.3. Electrical conductivity

The easiest and the most widely used technique to measure the sheet resistance (R_S) of a thin film is using the four-point probe (4pp) technique. Four evenly spaced, co-linear probes are utilized in a standard four-point probe instrument to make electrical contact with the substance being evaluated. During the measurement, a direct current (DC) was sent via the outer probes, allowing a voltage to be generated between the two inner probes. Eq. (1) will be used to compute the sheet resistance by measuring this potential difference between the probes. The sheet resistance, which was measured in [Ω/sq], would be helpful for analyzing thin conducting layers, the voltage drop measured across the inner probes labelled as ΔV, and I is the current applied at the outer probes.

Table 1
Metal deposition parameters for metallization process of adhesive layer of titanium and seed layer of copper.

Parameters	Titanium Target	Copper Target
Gas	Argon at 10 mTorr	Argon at 10 mTorr
Temperature	40°C	40°C
Deposition Duration	35 min	30 min

Table 2
Current density for copper electrodeposition process.

Sample	Current Density (mA) to %
S1	17.5 = 25 %
S2	35.0 = 50 %
S3	52.5 = 75 %
S4	70.0 = 100 %

Table 3
Sample classification after metallization process.

Group Sample	Current Density for Copper Plating (%)	Sample Name
S	25	S-25
	50	S-50
	75	S-75
	100	S-100

$$R_S = \frac{\pi}{\ln(2)} \frac{\Delta V}{I} = 4.53236 \frac{\Delta V}{I} \tag{1}$$

In this work, the sheet resistance measurements system from Jandel Four Point Probe (RM3000+, Leighton Buzzard, BEDS, UK) was used to evaluate the electrical resistance of thin metal layers. Later, Eq. (2) was used to determine the material's resistivity ρ, from the sheet resistance Rs, where tf is the thickness of the sheet being investigated.

$$R_S = \frac{\rho}{t_f} \tag{2}$$

During the measurement, the sample was placed in the holder and the probes were placed slowly to made contact with the film avoiding any damage to the coated surface. With a total of five locations per sample tested, a full substrate mapping was performed throughout the whole sample that been cut to 1 × 1 cm substrate in order to analyze the variance in sheet resistance across the films. The mean of the sheet resistance was computed. It was important to carefully specify the measurement sites on samples by focusing on distinct areas, including the center, top, bottom, left, and right, to enable reliable measurement process.

2.4. Surface morphology

The field-emission scanning electron microscope (FESEM) of JSM-IT800 SHL (JEOL) was used to study the surface morphology and the thickness of the coated substrate. The high-resolution micrograph from the FESEM allows for the unique topological feature of the coated surface to be identified. Accordingly, all surface morphological and topological information from coated surface (from macro- to nanoscale) will be analyzed to relate the effect of process parameters with the electrical conductivity and RF wave propagation on this works. Therefore, the thickness t_f, in Eq. (2) acquired from the FESEM's cross-section micrograph of coated metal (copper and titanium) will be used to calculate sample conductivity by using Eq. (3).

$$\text{Conductivity}, \ \sigma = \frac{1}{R_S \times t_f} \tag{3}$$

An optical-based surface profilometer is used to measure the three-dimensional morphology of a surface. It works by projecting a laser beam onto the surface of a sample, and measuring the reflected laser light as it bounces back off the surface. By analyzing the angle of reflection of the laser light, this technique can determine the topology of the sur-face with high precision. Profilometer LSM 700 (Jena, TLfDI, German) manufactured by Zeiss was used to investigate the surface topology of the sample.

2.5. Antenna design, fabrication and validation

In simple patch antenna design, it contains a few basic shapes which are rectangular sheets or "patches" of the conductive layer on top of a dielectric substrate then supported by a larger conductive layer called ground as shown in Fig. 3. The microstrip patch antennas are usually rectangular or oval, but they can be made in any suitable geometrical form. One of the most important considerations in wave propagation of the antennas is the resonance frequency that depend of the dimension of the patch layer [39]. To design a patch antenna, the dimension can be calculated with Eq. (4) [40,41].

$$\text{Width, } W = \frac{c}{2f_0}\sqrt{\frac{2}{\varepsilon_r+1}} \tag{4}$$

Where c is the speed of light, f_0 is the resonant frequency, and ε_r is the dielectric constant of the substrate. Effective dielectric constant can be determined using Eq. (5).

$$\varepsilon_{ref} = \frac{\varepsilon_r+1}{2} + \frac{\varepsilon_r-1}{2}\left[\frac{1}{\sqrt{1+12\frac{h}{W}}}\right] \tag{5}$$

Where ε_{reff} is the effective dielectric constant, h is the thickness of the antenna. Due to fringing effects, the size of the antenna is increased by an amount of (ΔL). Therefore, the extension of the length (ΔL) of the patch is to be calculated using Eq. (6).

$$\Delta L = 0.412h\left(\frac{(\varepsilon_{reff}+0.3)\left(\frac{w}{h}+0.264\right)}{(\varepsilon_{reff}-0.258)\left(\frac{w}{h}+0.8\right)}\right) \tag{6}$$

The actual length of the patch can now be determined using Eq. (7).

$$\text{Length, } L = \frac{c}{2f_0\sqrt{\varepsilon_{reff}}} - 2\Delta L \tag{7}$$

The antenna in this study was meant to be a reconfigurable patch antenna with different frequencies of 2.4 GHz, 3.5 GHz, and 5GHz. Fig. 4 (a) depicts the antenna's dimension and assembly, which will be built on a Lego-like structure with poles and holes. An antenna, as shown in Fig. 4(b), has three radiating patch designs for three different frequencies and one ground structure. As a result, all three patch designs have the same ground structure.

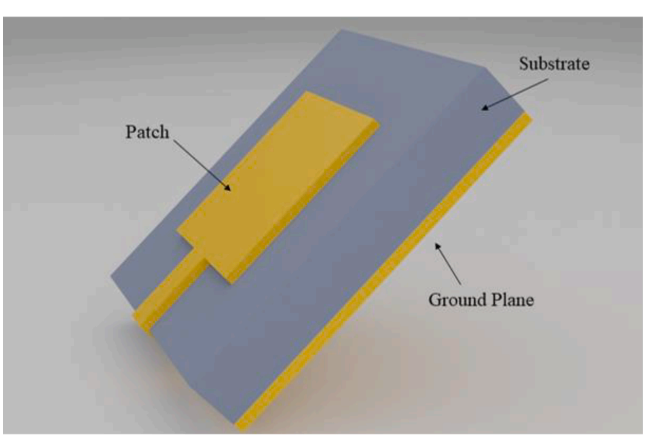

Fig. 3. The illustration of patch antenna basic structure.

The patch antenna was simulated in Ansys HFSS software, which utilized a 3D full-wave Finite Element Method (FEM) to compute the wave propagation behavior of complex components of arbitrary shape and user-defined material properties. The simulation yielded the antenna's reflection coefficient and radiation pattern. Once the simulation was completed, the antenna was modelled in 3D CAD software called Blender. The modeled design would be subsequently converted into standard triangulated language (STL) file and sliced with Formlabs' Preform Slicer. The sliced design of STL file was printed using a Form 2 3D printer manufactured by Formlabs using High Temperature V2 resin. Further curing was followed using Form Cure for 60 min. As illustrated in Fig. 5, the antenna was constructed with an additional thickness of 0.2 mm for the metallization process, which was subsequently polished to remove undesired structure and produce the desired patch structure. Damascene-like technique was used to describe this approach [5]. The antennas were characterized using a vector network analyzer (Anritsu MS2024B VNA Master, Atsugi, OL, Japan). VNA was used to determine the S-parameter of an antenna, which are important parameters for determining the efficiency of an antenna. Before measuring the reflection coefficient of the fabricated antennas, the calibration for measurement setup was applied using calibration kit and standard antenna supplied by the manufacturer. Fig. 6 illustrated the final antenna equipped with male SMA connector attached to a female coax cable for antenna characterization.

3. Results and discussion

3.1. Electrical conductivity

The electrical performance of the deposited copper layer was studied from conductivity measurement. The sample conductivity was shown in Fig. 7 and compared with conductivity from standard copper metal. When the current density was increased during the electrodeposition process, the conductivity value for the sample increased in mixed-nonlinear trends. The samples S-25 with a current density of 25 % show the lowest conductivity value of 4.59 MS/m, whereas the samples S-50 and S-75 exhibited an increase of conductivity value from 6.27 MS/m and 19.7 MS/m respectively. Meanwhile, the samples of S-100 showed only a marginal conductivity value compared to S-75 at 22.4 MS/m. The full coalescence of the isolated copper particle could be responsible for the sharp increase in the conductivity between current density of 50 % and 75 %, on the contrary at maximum 100 % the copper ions were infused rapidly filling-up the voids. Typically, the electrolyte of the electrodeposition process can easily penetrate the void thus capable to improve the deposition of the metal producing a continuous layer, which later would greatly enhance the electrical conductivity of the deposited metal hence a new electrical paths were created [42]. Comparatively, the conductivity of copper (58 MS/m) from International Annealed Copper Standard (IACS) was included in Fig. 8. As indicated, at maximum current density of 70 mA per square inch, this electrodeposition process was only reached to about 39 % from the standard copper for 30 min deposition duration. According to Darvishzadeh et al., by increasing the deposition duration longer at marginal current density between 50 and 75 % could further enhanced conductivity of the final copper layer [43].

The electrodeposition process such as sputtering and electroplating could be complex and time-consuming, requiring precise control of parameters like current density and the duration of metal deposition [44]. Therefore, the optimized parameter for sputtering had been set up as mentioned earlier. However, the sputtering process could not provide an optimum conductive metal layer because the antenna required a certain skip depth to reduce the attenuation in practical applications [45]. Therefore, an additional process of electroplating copper was to provide a smoother surface of conductive metal layer. Other than that,

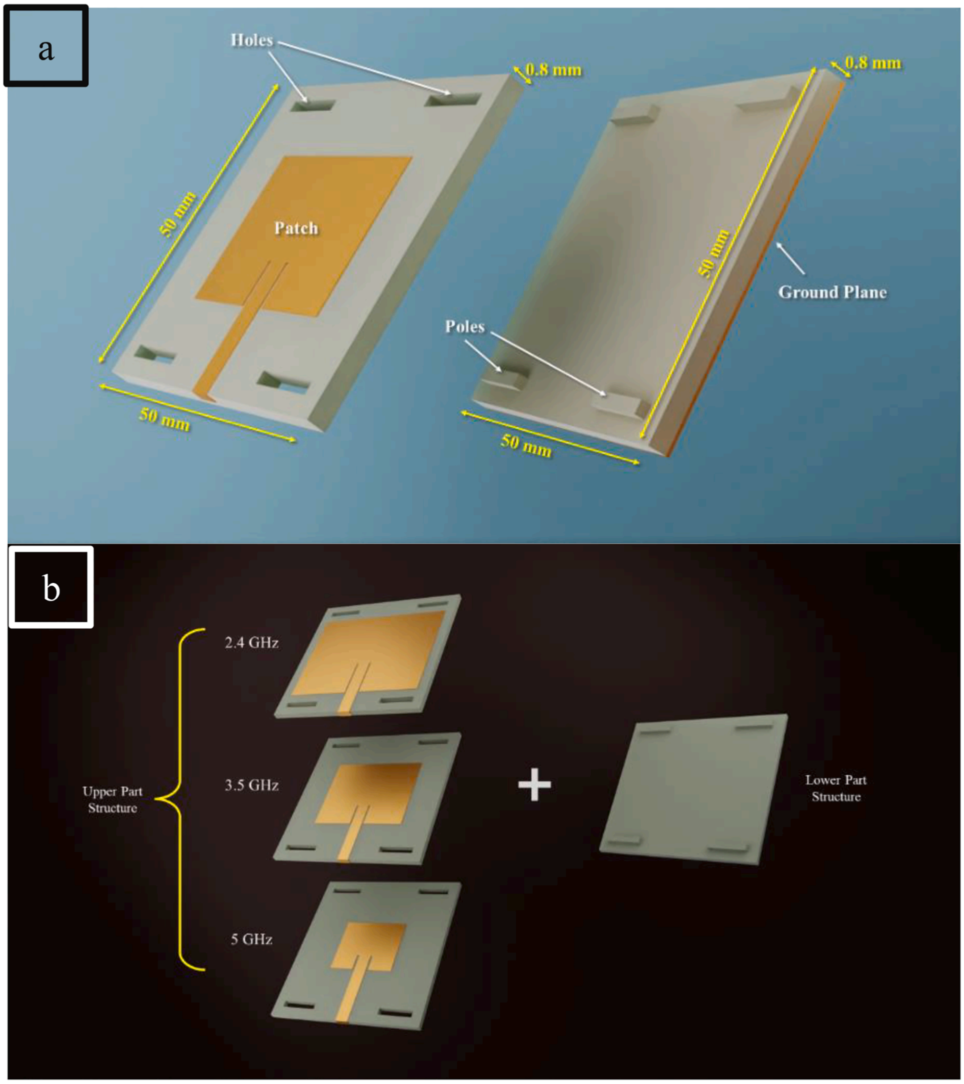

Fig. 4. (a) A Lego-like structure for the reconfigurable patch antenna applied in this study; (b) Patch design for three different frequencies with the same ground structure.

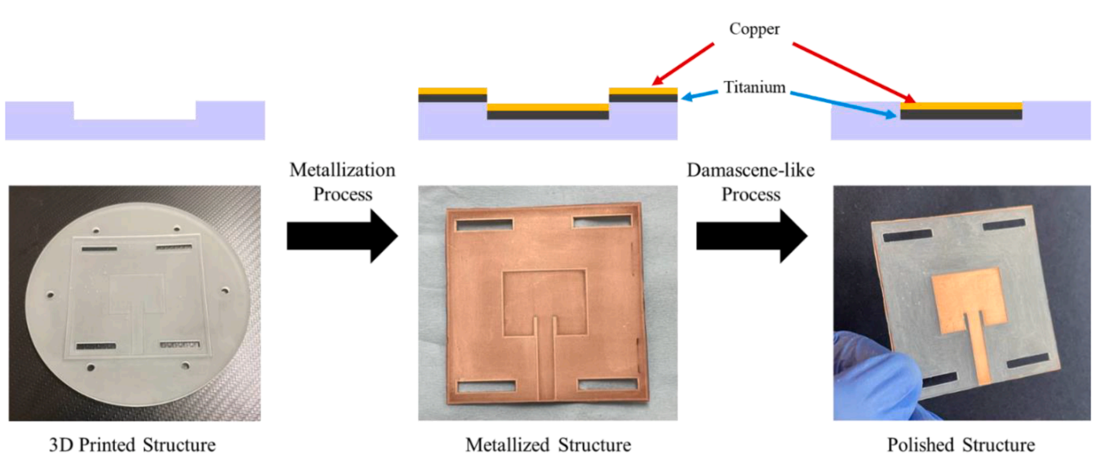

Fig. 5. A damascene-like technique was used to achieve the desired pattern after the metallization procedure.

the surface roughness of conductive metal layer must be uniform to ensure the wave could propagate efficiently and ensure that the antenna resonated at precise frequency that later would be further discussed in the FESEM and surface roughness section [34]. The most significant factors that affected the uniformity of copper layer was the precision of 3D printed substrate. The limitation of 3D printer could also contributed towards uneven thickness of surface 3D printed substrate at the first place before sputtering and electroplating processes. Table 4 shows the

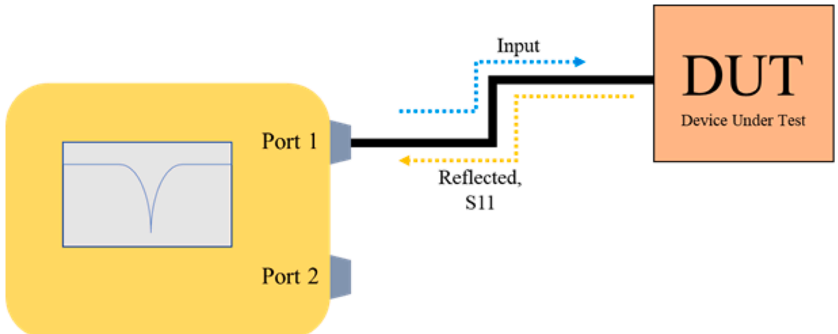

Fig. 6. An illustration of experiment setup used for reconfigurable patch antenna characterization.

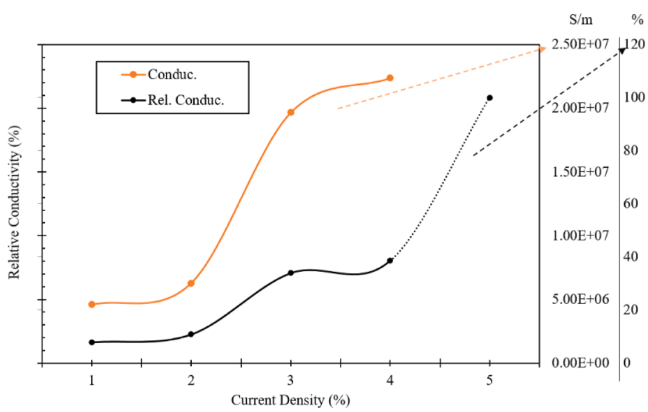

Fig. 7. The conductivity of the samples at different current density.

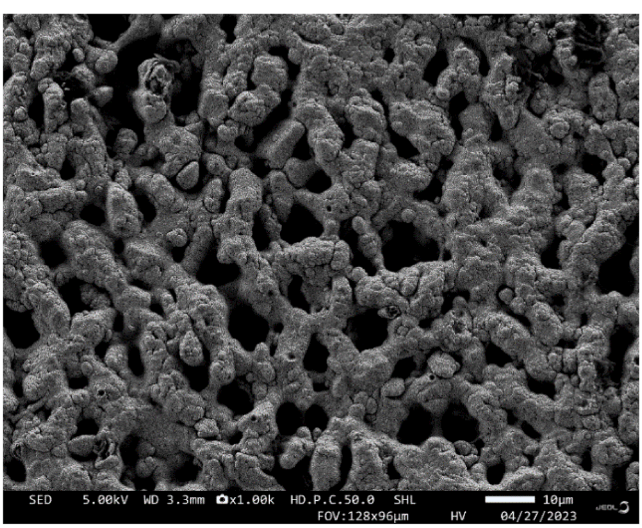

Fig. 8. FESEM micrographs of the 3D printed substrate surface after the sputtering process only.

electrical resistivity of different techniques of deposition metal layer on varied substrates for a comparison between our work and past studies.

3.2. *Field emission scanning electron microscopy (FESEM)*

Fig. 8 shows FESEM microphotographs of sputtered copper on the 3D printed surface of a substrate with magnification of × 1000, meanwhile Fig. 9(a-d) display FESEM microphotographs of dual metallization approach whereas sputtered and electroplated copper. Fig. 9(e) has a lot of pores due to the 3D printing process. From the image analysis using ImageJ, the pore size was in the range of 10 μm, potently increased the electrical surface resistance of the sputtered copper layers. According to the technical specification from the manufacturer of Form 2 SLA 3D printer, the laser spot size (FWHM) was about 140 μm, but finer tuning and optimization during slicing process had capable to improve the quality of printed substrate. On the other hand, Fig. 8(a-d) displayed the deposited copper layer on the surface of the substrate at various applied current densities, consists of 25 %, 50 %, 75 %, and 100 % for S-25, S-50, S-75, and S-100, respectively, at deposition duration of 30 min. A continuous and consistent layer of copper was visible along the surface, as shown in Fig. 9(a-b) when current density was increased from 25 % to 50 %. Thus, the observed copper layer indicated that the electrodeposition copper process was able to fill up the pores which later led to improve of electrical surface resistance of the copper layers. As the current density increased further from 75 % to 100 %, the ability of the copper ions from electrodeposition process to fill-up the empty pores somehow not consistent as shown in Fig. 9(c-d). Reasonably, the deposition rate of copper should increase linearly with an increase in applied current, practically smoothing out the holes on the substrate surface. Statistical and experimental work by Darvishzadeh et al. studied the influence of current density and deposition duration on fabric surface discovered the optimal condition for uniform surface morphology which significantly enhanced the electrical conductivity of deposited metal [43]. Metal deposition using electrodeposition process govern by several mechanisms, such as nucleation, growth, and coalescence of metal particle that strongly depend on these two parameters [48,49]. It was found that the morphology of the deposited metal changed to a non-uniform structure when the deposition were done at high current density and rapid growth [50]. Therefore, the formation of micro-cluster on the surface was obtained when the electrical current density was in the range of 50 % to 75 % as shown in Fig. 9(b-c). Further increased to maximum 100 % (70 mA) caused the copper layer to become rougher due the higher deposition kinetic suffered by copper ions in the electrolyte [51].

Table 4
The electrical resistivity of copper layer deposited onto varied of substrates.

Methods	Conductive Layer	Substrate	Electrical Resistivity (Ω·cm)	Ref.
Doctor-blade	Copper paste	Polyethylene terephthalate (PET)	240×10^{-6}	[46]
Screen printing	Copper ink	Polyimide film	12.5×10^{-6}	[47]
Sputtering and Electroplating (Dual Metallization)	Copper	3D printed substrate (High Temperature Resin)	9.97×10^{-3}	Our work

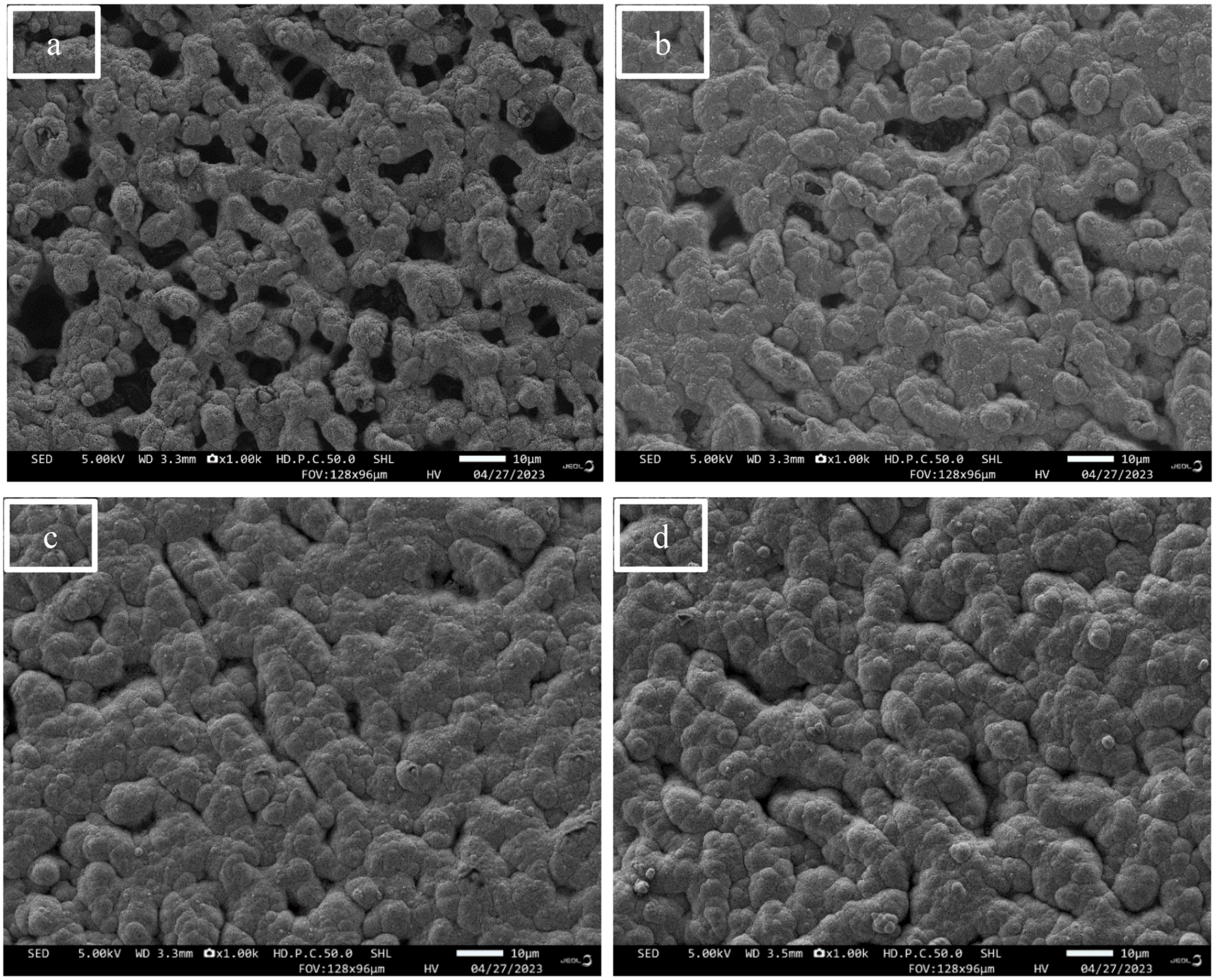

Fig. 9. FESEM micrographs of the 3D printed substrate surface after sputtering and electroplating processes for different current density rated from 70 mA: a) 25 %; b) 50 %; c) 75 % and d) 100 %.

3.3. Surface roughness

The sample surface quality from electrodeposition process was determined using optical profiler technique. The average mean height (Sa) was used to relate the effect between current density and the surface morphology of the samples. From the electrical conductivity result, more pores and flaws were established during the electrodeposition process as the current density surpassed the recommended threshold, consistent with many other findings [42,49,50,52]. From Fig. 10(a) and 10(d) for sample S-25 and S-100 respectively, showed an uneven surface with a lot of pores compared to sample S-50 and S-75 displayed by Fig. 10(b) and Fig. 10(c) respectively. Clearly, sample S-75 has the best and the smoothest surface as most pores have been covered compared to all samples. Rohini et al. and Li et al. observed from the FESEM micrographs and optical images, the deposited metal deformed from spherical shape to cones shape at higher current density producing a non-uniform and rougher surface [53,54]. Therefore, the complex kinetic and dynamic nature of metal deposition must be carefully assessed to ensure the optimal surface quality using electroplating technique.

Fig. 11 showed the surface roughness of the samples at different current densities. The average mean height (Sa) for sample with current density of 75 % has the smallest value among others but sample with current density of 100 % show marginal increase of the mean height value. Lower surface roughness of the sample could be achieved by using less current density compared to the sample with 100 % of current density. The surface roughness of the 3D printed structure was one of the limitations in fabrication of antenna. According to Wang et al., a rough surface could substantially reduce the electromagnetic performance in terms of increased conduction loss [32]. Higher surface roughness would cause amplitude and phase errors of the radiating slot, thus decreasing the gain and efficiency of the patch antenna [55].

3.4. Application of patch antenna

In this section, the initial performance of the fabricated 3D printed patch antennas are shown. The measured reflection coefficient results for 2.4 GHz antenna design as depicted in Fig. 12(a) shows that the antenna resonance at 2.56 GHz with maximum return loss of 31.30 dB Fig. 12(b) shows the 3D printed patch antenna specifically designed for 2.4 GHz frequency. Based on the results of the measurements, the patch's 10-dB return-loss bandwidth was found to be 0.126 GHz. The measured reflection coefficient of the antenna radiates at a difference of 0.16 GHz from the simulated measurement. Fig. 12(c) and Fig. 12(d) show the simulated and measured reflection coefficient of the proposed antenna for 3.5 GHz and the fabricated structure of the antenna respectively. The operational frequency of the measured antenna was at 3.68 GHz, slightly higher by 0.18 GHz from the simulated frequency and has a bandwidth of 0.275 GHz. The subsequent antenna, designed for 5 GHz, displayed a minor discrepancy in its performance, with the measured operational frequency transmitting at 5.33 GHz and a

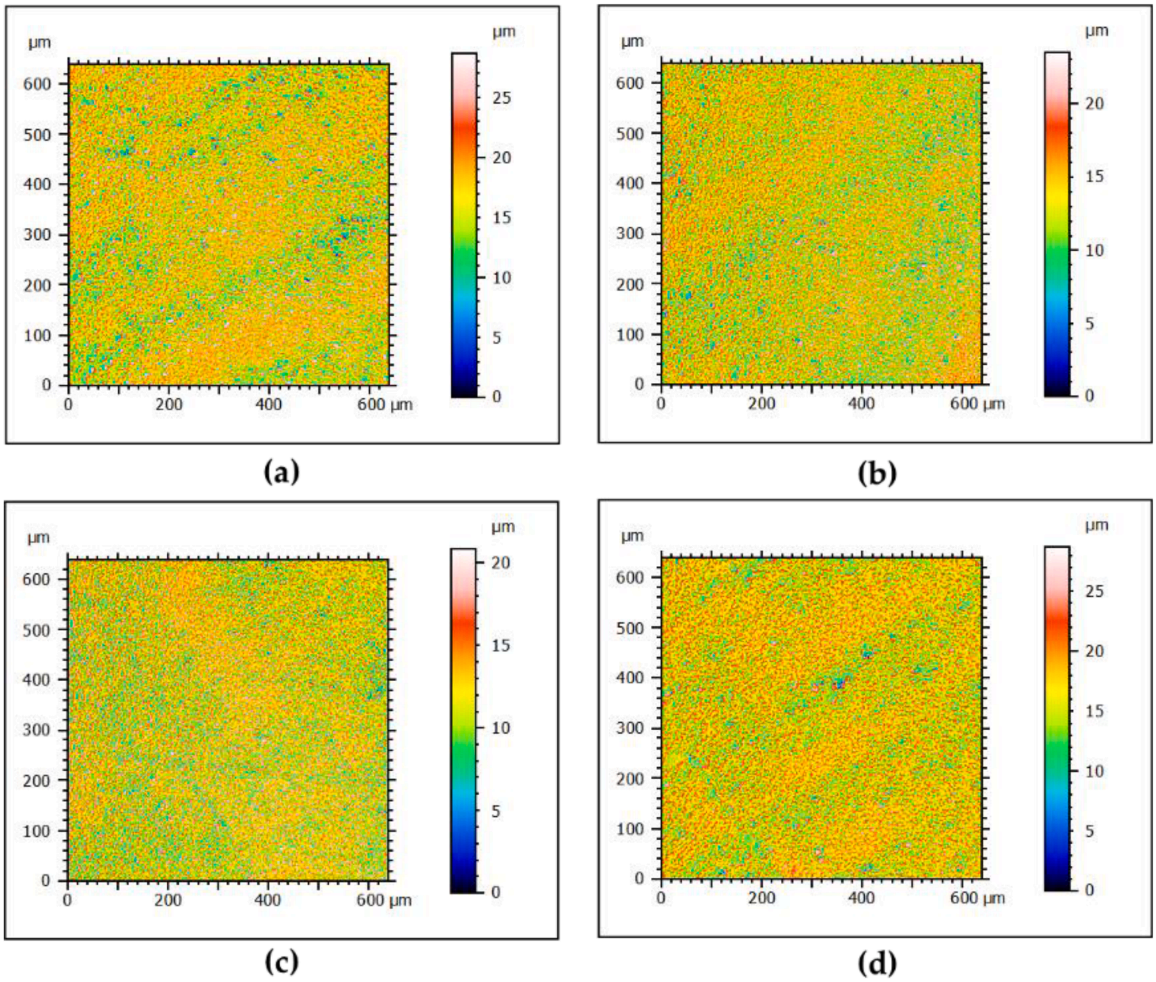

Fig. 10. Surface morphologies of the sample for (a) 25 %, (b) 50 %, (c) 75 %, and (d) 100 % of current density.

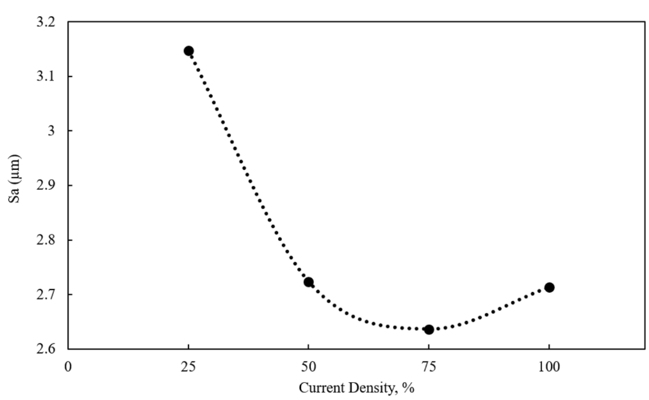

Fig. 11. Surface roughness (Sa) of the samples.

maximum return loss of 25.18 dB, as depicted in Fig. 12(e) with the bandwidth of 0.33 GHz. Fig. 12(f) displays the 5 GHz antenna, which was fabricated utilizing 3D printing technology.

The discrepancy observed in the operational frequency between the simulated and measured antenna could primarily be attributed to various factors related to the assembly process which subsequently alter the antenna's performance characteristics. This factor might be due to the mechanical integration of the antenna lower and upper 3D printed structure which was joined via LEGO-like interlocking technique as depicted in Fig. 13. In addition, this assembly method resulted in additional series resistance from the conductive silver paste, surface abrasion and the presence of slight air gaps. The presence of the air gap between the substrates occurred due to the waviness and the roughness on the surface of the substrate during the printing process. Moreover, the substrate experienced warping during the metallization process due to exposure to heat. This introduced stress to the copper layer, leading to imperfections in the antenna structure, further contributing to the air gaps formation.

The air gap caused the actual dielectric of the antenna to be slightly different compared to the initial dielectric, ε_r of the substrate. Actual dielectric can be calculated using derivation of the Eq. (8). From the equation, a new simulation has been done to prove the antenna matching between simulation and the actual antenna. There was a good agreement between the actual measurement and the simulated measurement of the antenna as shown in Figs. 14–16 for 2.4 GHz, 3.5 GHz, and 5 GHz antenna design respectively.

$$\text{Width} = \frac{c}{2f_o\sqrt{\frac{\varepsilon_R+1}{2}}}$$

$$2f_o \times \text{Width} = \frac{c}{\sqrt{\frac{\varepsilon_R+1}{2}}}$$

$$\sqrt{\frac{\varepsilon_R+1}{2}} = \frac{c}{2f_o \times \text{Width}}$$

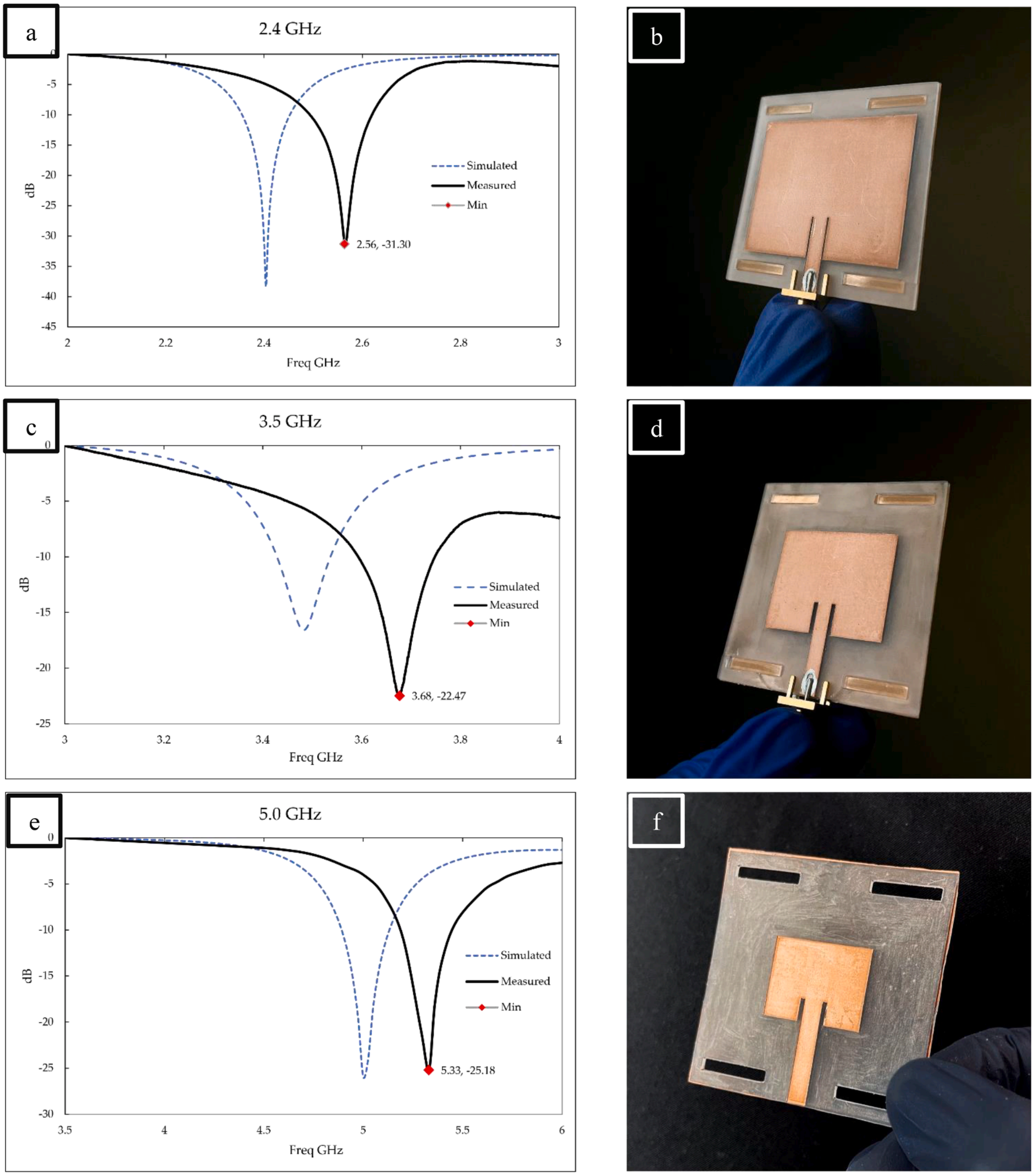

Fig. 12. A Comparison of the reflection coefficient between measured reconfigurable patch antenna using VNA with the simulated performance from Ansys HFSS for (a-b) 2.4 GHz, (c-d) 3.5 GHz, and (e-f) 5 GHz design.

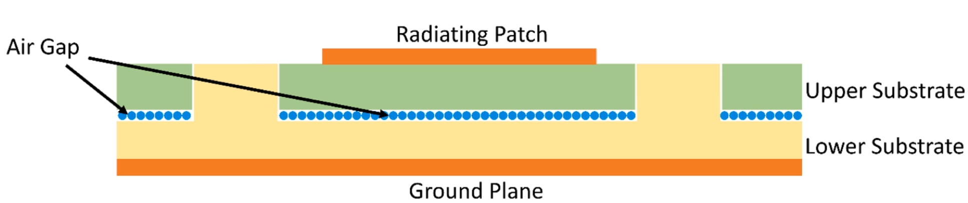

Fig. 13. The illustration of an air gap between substrates.

$$\frac{\varepsilon_R + 1}{2} = \left(\frac{c}{2f_o \times \text{Width}}\right)^2 \qquad \varepsilon_R = \left[\left(\frac{c}{2f_o \times \text{Width}}\right)^2 \times 2\right] - 1 \tag{8}$$

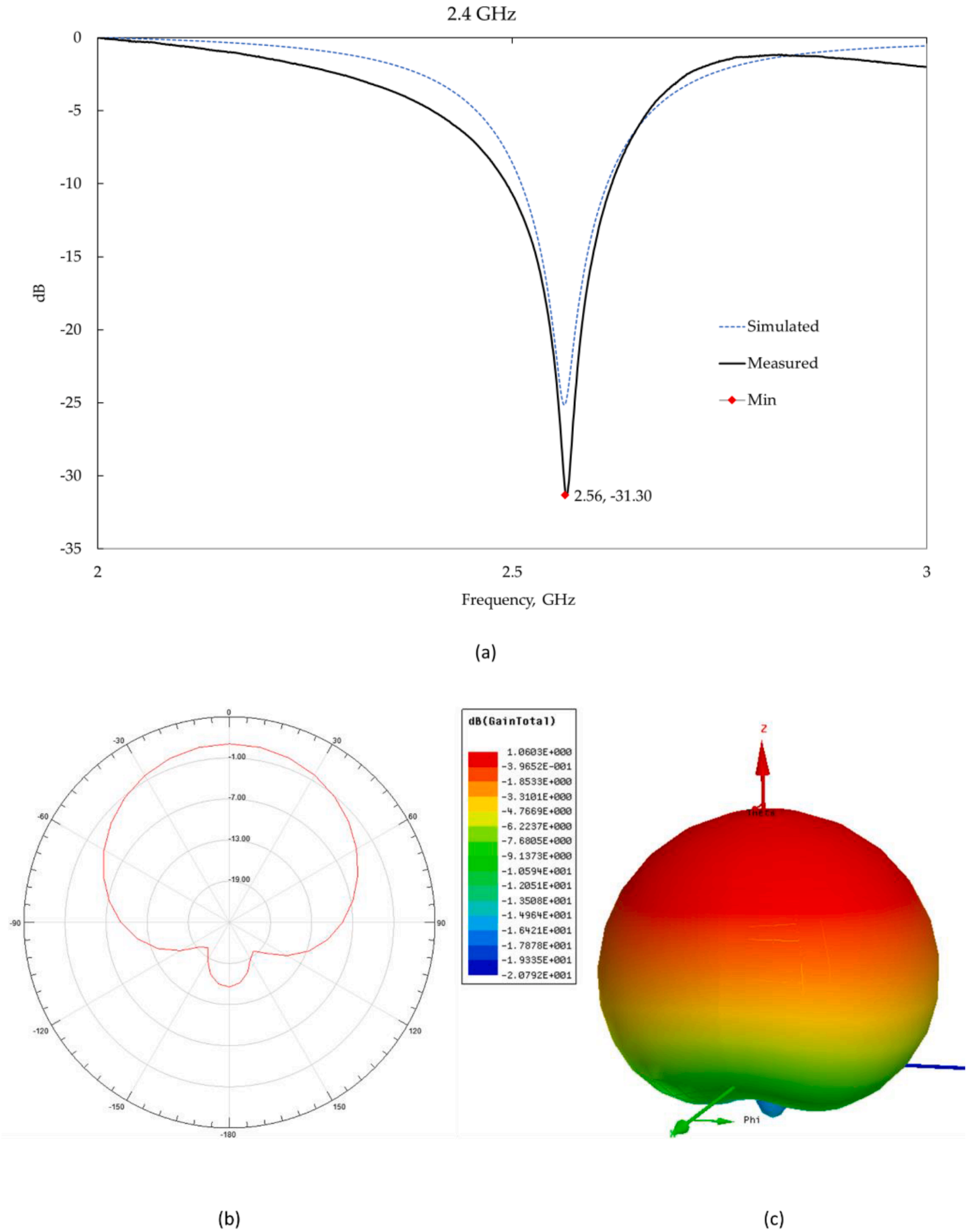

Fig. 14. (a) Simulated and measured reflection coefficient for 2.4 GHz antenna design; (b) Radiation pattern of the antenna simulation; (c) 3D radiation pattern of the antenna.

4. Conclusion

Fabrication of the reconfigurable patch antenna for different frequencies at 2.4 GHz, 3.5 GHz, and 5 GHz using additive manufacturing method were demonstrated. A stereolithography 3D printer with a very fine resolution up to 0.01 mm layer height allows the fabrication of patch antenna that operated at good performance level. This works provided an experimental and analysis of the most suitable current density for the electrodeposition process for the 3D printed substrate for conductive layer. Different current density for electrodeposition process were ranging from 25 % to 100 % of 70 mA. The most suitable current density was obtained at 75 % as it showed the best surface quality compared to others without compromising the electrical conductivity of copper layers.

3D printing technology allowed new patch antenna designs to be reconfigurable without changing the entire structure of the antenna, resulting in cost and material savings. By creating antenna design constructed with Lego-like structure, the reconfigurable patch antenna

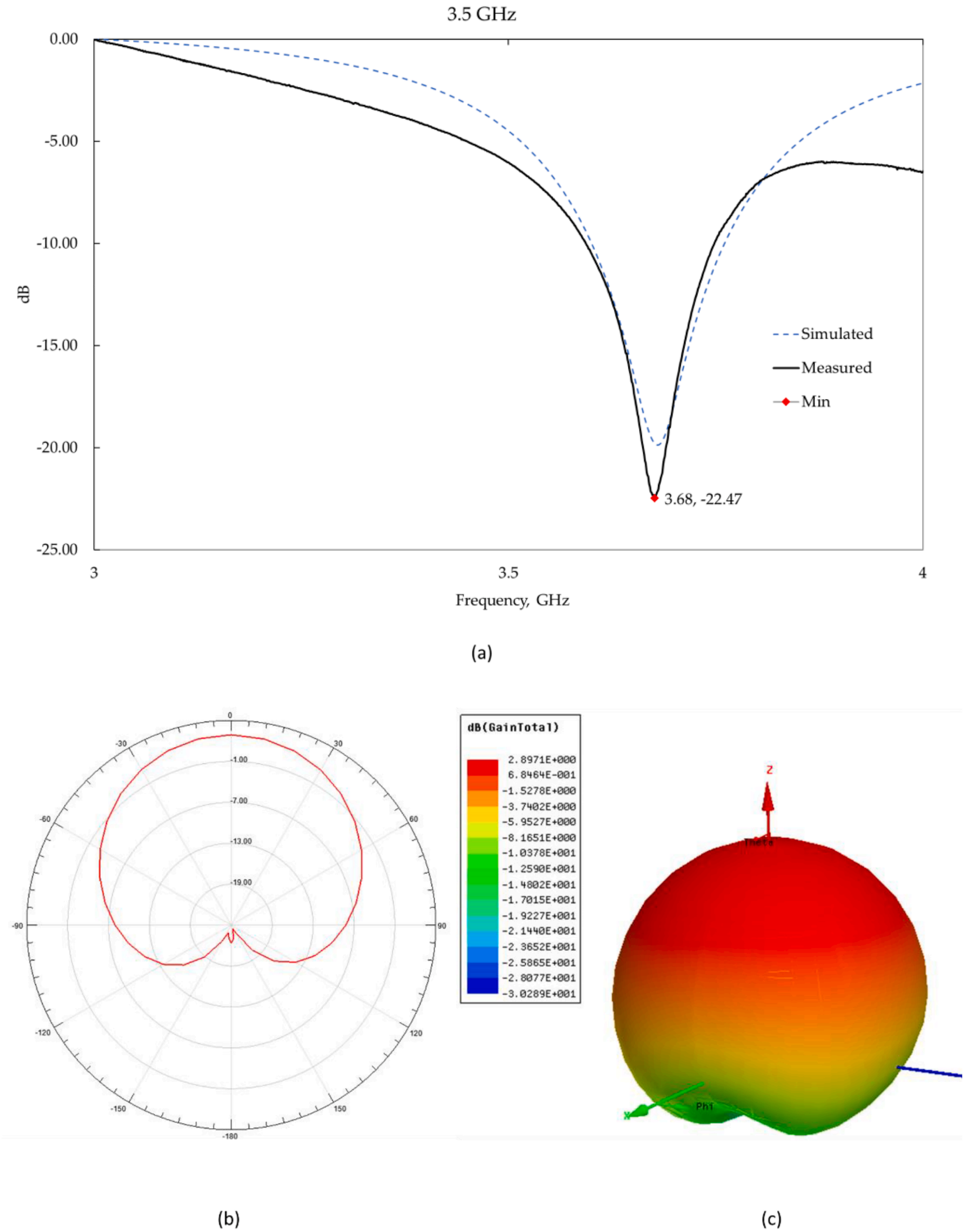

Fig. 15. (a) Simulated and measured reflection coefficient for 3.5 GHz antenna design; (b) Radiation pattern of the antenna simulation; (c) 3D radiation pattern of the antenna.

design could be achieved as demonstrated in this works. The antenna was then measured using VNA and the discrepancy between measured and the simulated performance were ranging from 0.1 GHz until 0.33 GHz. The difference of the value between the simulated and measured antenna might be due to the air gap between the ground part and upper part (patch antenna). The air gap occurred because of the waviness, surface roughness, and the printed parts warped due to heat exposure during sputtering process. Overall, reconfigurable patch antenna could be developed using additive manufacturing techniques and allowed a new antenna design for the patch antenna which leads to cost reduction. This would open an opportunity for the researcher to be more flexible in designing and fabricating more design of patch antennas at low cost and manufacturing the antennas would be much easier than before.

Funding

This research was supported by the Fundamental Research Grant Scheme (FRGS) (Investigation of Low Cost Substrate-Based Antenna

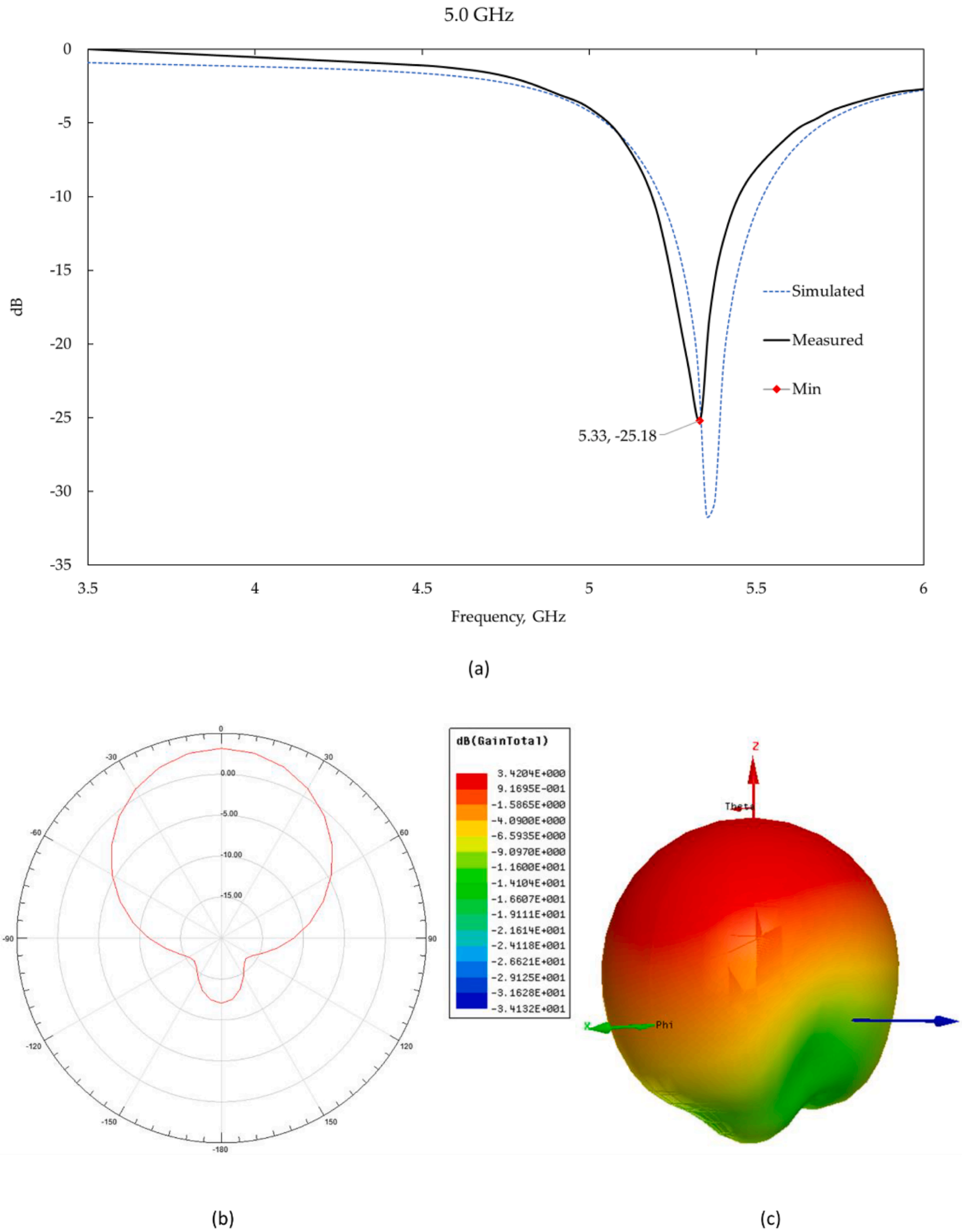

Fig. 16. (a) Simulated and measured reflection coefficient for 5 GHz antenna design; (b) Radiation pattern of the antenna simulation; (c) 3D radiation pattern of the antenna.

Using Three-Dimensional Printing Technology for Fifth Generation Wireless System) –FRGS/1/2021/TK0/UTM/02/60) awarded by the Ministry of Education of Malaysia. The corresponding author also wishes to acknowledge Ministry of Higher Education of Malaysia (MOHE) and Universiti Sains Islam Malaysia (USIM) for the scholarship (KPT(BS) 880,123) to pursue postdoctoral research fellow at University of Cambridge, UK.

CRediT authorship contribution statement

Ahmad Nurhelmy Adam: Writing – review & editing, Writing – original draft, Visualization, Methodology, Investigation, Formal analysis, Conceptualization. **Irfan Yahaya:** Methodology, Investigation, Formal analysis, Conceptualization. **Ahmad Adnan Abu Bakar:** Writing – review & editing. **Shahino Mah Abdullah:** Validation, Supervision. **Nizam Tamchek:** Writing – review & editing, Validation, Supervision, Resources, Project administration. **Ahmad F. Alforidi:** Validation. **Ahmed Alahmadi:** Validation. **Mohd Haizal Jamaluddin:** Resources, Funding acquisition. **Mohd Azraie Mohd Azmi:** Supervision. **Mohd Ifwat Mohd Ghazali:** Writing – review & editing, Validation, Supervision, Resources, Project administration, Funding acquisition, Conceptualization.

Declaration of competing interest

The authors declare that they have no known competing financial interests or personal relationships that could have appeared to influence the work reported in this paper.

Acknowledgements

This research was supported by the Fundamental Research Grant Scheme (FRGS) (Investigation of Low Cost Substrate-Based Antenna Using Three-Dimensional Printing Technology for Fifth Generation Wireless System) –FRGS/1/2021/TK0/UTM/02/60) awarded by the Ministry of Education of Malaysia. The corresponding author also wishes to acknowledge Ministry of Higher Education of Malaysia (MOHE) and Universiti Sains Islam Malaysia (USIM) for the scholarship (KPT(BS) 880123) to pursue postdoctoral research fellow at University of Cambridge, UK.

Data availability

No data was used for the research described in the article.

References

[1] S. Rouf, A. Malik, N. Singh, A. Raina, N. Naveed, M.I.H. Siddiqui, M.I.U. Haq, Additive manufacturing technologies: industrial and medical applications, Sust. Oper. Comput. 3 (2022) 258–274, https://doi.org/10.1016/j.susoc.2022.05.001.

[2] A.A. Abu Bakar, M.Z. Zainuddin, A.N. Adam, I.S. Mohd Noor, N. Tamchek, M. S. Alauddin, M.I. Mohd Ghazali, The study of mechanical properties of poly(lactic) acid PLA-based 3D printed filament under temperature and environmental conditions, Materials Today 67 (2022) 652–658, https://doi.org/10.1016/j.matpr.2022.06.198.

[3] M.Z. Zainuddin, A.A. Abu Bakar, A.N. Adam, S.M. Abdullah, N. Tamchek, M. S. Alauddin, M.M. Mahat, N. Wiwatcharagoses, A. Alforidi, M.I.M. Ghazali, Mechanical and Structural Properties of Polyhydroxybutyrate as Additive in Blend Material in Additive Manufacturing for Medical Applications, Polymers (Basel) 15 (2023), https://doi.org/10.3390/polym15081849.

[4] S.A.M. Tofail, E.P. Koumoulos, A. Bandyopadhyay, S. Bose, L. O'Donoghue, C. Charitidis, Additive manufacturing: scientific and technological challenges, market uptake and opportunities, Mater. Today 21 (2018) 22–37, https://doi.org/10.1016/j.mattod.2017.07.001.

[5] M.I.M. Ghazali, S. Karuppuswami, A. Kaur, P. Chahal, 3-D Printed Air Substrates for the Design and Fabrication of RF Components, IEEE Trans. Components Packaging Manufact. Technol. 7 (2017) 982–989, https://doi.org/10.1109/TCPMT.2017.2686706.

[6] H. Xin, M. Liang, 3D Printed Microwave and Jetting Techniques THz Devices Using Polymer, Proc. IEEE (2016) 1–19.

[7] R. Kudelski, J. Cieslik, M. Kulpa, P. Dudek, K. Zagorski, R. Rumin, Comparison of cost, material and time usage in FDM and SLS 3D printing methods, in: 2017 XIIIth International Conference on Perspective Technologies and Methods in MEMS Design (MEMSTECH), 2017, pp. 12–14, https://doi.org/10.1109/MEMSTECH.2017.7937521.

[8] N.K. Das, Antennas and Radiation, The Electrical Engineering Handbook (2004) 569–583. https://doi.org/10.1016/B978-012170960-0/50043-8.

[9] M.I.M. Ghazali, E. Gutierrez, J.C. Myers, A. Kaur, B. Wright, P. Chahal, Affordable 3D printed microwave antennas, in: 2015 IEEE 65th Electronic Components and Technology Conference (ECTC), 2015, pp. 240–246, https://doi.org/10.1109/ECTC.2015.7159599.

[10] C.A. Reynaud, D. Duché, J.J. Simon, E. Sanchez-Adaime, O. Margeat, J. Ackermann, V. Jangid, C. Lebouin, D. Brunel, F. Dumur, D. Gigmes, G. Berginc, C.A. Nijhuis, L. Escoubas, Rectifying antennas for energy harvesting from the microwaves to visible light: a review, Prog. Quantum Electron. 72 (2020), https://doi.org/10.1016/j.pquantelec.2020.100265.

[11] A. Dadgarpour, A. Abbosh, F. Jolani, Planar multiband antenna for compact mobile transceivers, IEEE Antennas Wirel. Propag. Lett. 10 (2011) 651–654, https://doi.org/10.1109/LAWP.2011.2159696.

[12] R.H. Mahmud, I.H. Salih, X. Shang, T. Skaik, Y. Wang, A filtering waveguide aperture antenna based on all-resonator structures, Microw. Opt. Technol. Lett. 65 (2023) 2378–2383, https://doi.org/10.1002/mop.33706.

[13] T.H. Gan, A. Liu, P.K. Tan, J. Lu, A Bendable Wideband Dual-Polarization Conformal Phased-Array Antenna, IEEE Antennas Wirel. Propag. Lett. 22 (2023) 1952–1956, https://doi.org/10.1109/LAWP.2023.3270431.

[14] Y. Cheng, Y. Dong, High-Gain All-Metal 3-D Printed Lens–Horn Antenna for Millimeter-Wave Applications, IEEE Antennas Wirel. Propag. Lett. 22 (2023) 308–312, https://doi.org/10.1109/LAWP.2022.3209788.

[15] S. Rezaeeahvanouee, D. Dehmeshki, Y. Tousi, Theoretical Study and Systematic Design of Multiport Wire Antenna, IEEE Antennas Wirel. Propag. Lett. 22 (2023) 2270–2274, https://doi.org/10.1109/LAWP.2023.3283448.

[16] K.A. Fante, M.T. Gemeda, Broadband microstrip patch antenna at 28 GHz for 5G wireless applications, Int. J. Electri. Comput. Eng. 11 (2021) 2238–2244, https://doi.org/10.11591/ijece.v11i3.pp2238-2244.

[17] P. Reis, H.G. Virani, Design of a Compact Microstrip Patch Antenna of FR-4 Substrate for Wireless Applications, in: 2020 International Conference on Electronics and Sustainable Communication Systems (ICESC), 2020, pp. 713–716, https://doi.org/10.1109/ICESC48915.2020.9156024.

[18] R.H. Thaher, H.M. Jassim, Design of dual band elliptical microstrip antenna for satellite communication, IOP Conf. Series 928 (2020), https://doi.org/10.1088/1757-899X/928/2/022066.

[19] H.R. Heidari, P. Rezaei, S. Kiani, M. Taherinezhad, A monopulse array antenna based on SIW with circular polarization for using in tracking systems, AEU - Int. J. Electron. Commun. 162 (2023) 154563, https://doi.org/10.1016/j.aeue.2023.154563.

[20] S. Maiti, S.K. Rajak, A. Mukherjee, Design of a compact ultra wide band microstrip patch antenna, in: 5th International Conference on Computing Communication and Networking Technologies, ICCCNT 2014 2, 2014, pp. 11–13, https://doi.org/10.1109/ICCCNT.2014.6963083.

[21] S. Kiani, P. Rezaei, M. Fakhr, On-chip coronavirus shape antenna for wide band applications in terahertz band, J. Optics (India) 52 (2023) 860–867, https://doi.org/10.1007/s12596-022-01048-y.

[22] M.I. Mohd Ghazali, S. Karuppuswami, A. Kaur, P. Chahal, 3D Printed high functional density packaging compatible out-of-plane antennas, Addit. Manuf. 30 (2019) 100863, https://doi.org/10.1016/j.addma.2019.100863.

[23] S.M. Palhade, S.P. Yawale, Design and Photo-Lithographic Fabrication of Microstrip Patch Antenna, Int. J. Sci. Res. (IJSR) 4 (2015) 2021–2024. https://www.ijsr.net/getabstract.php?paperid=SUB151708.

[24] H. R., H. M., A. I., Design, Fabrication, and Testing of Flexible Antennas, Advancement in Microstrip Antennas with Recent Applications (2013). https://doi.org/10.5772/50841.

[25] M.I.M. Ghazali, E. Gutierrez, J.C. Myers, A. Kaur, B. Wright, P. Chahal, Affordable 3D printed microwave antennas, in: 2015 IEEE 65th Electronic Components and Technology Conference (ECTC) 2015-July, 2015, pp. 240–246, https://doi.org/10.1109/ECTC.2015.7159599.

[26] D. Helena, A. Ramos, T. Varum, J.N. Matos, The use of 3d printing technology for manufacturing metal antennas in the 5 g/iot context, Sensors 21 (2021), https://doi.org/10.3390/s21103321.

[27] Z. Li, J. Huang, Y. Yang, S. Yang, J. Zhang, P. Yuan, J. Zhang, Additive manufacturing of conformal microstrip antenna using piezoelectric nozzle array, Appl. Sci. (Switzerland) 10 (2020), https://doi.org/10.3390/app10093082.

[28] R. Colella, F.P. Chietera, L. Catarinucci, Analysis of FDM and DLP 3D-Printing Technologies to Prototype Electromagnetic Devices for RFID Applications, Sensors (Switzerland) 21 (2021) 1–13, https://doi.org/10.3390/s21030897.

[29] S.G. Kirtania, A.W. Elger, M.R. Hasan, A. Wisniewska, K. Sekhar, T. Karacolak, P. K. Sekhar, Flexible antennas: a review, Micromachines (Basel) 11 (2020), https://doi.org/10.3390/mi11090847.

[30] H. Agrawaal, J.E. Thompson, Additive manufacturing (3D printing) for analytical chemistry, Talanta Open 3 (2021) 100036, https://doi.org/10.1016/j.talo.2021.100036.

[31] J.M. Jafferson, H. Vinu, K. Sekaran, A study of additive manufacturing technologies and metallizing techniques for microwave waveguide components, Mater. Today 46 (2021) 1328–1334, https://doi.org/10.1016/j.matpr.2021.02.420.

[32] Y. Wang, X. Zhang, R. Su, M. Chen, C. Shen, H. Xu, R. He, 3D Printed Antennas for 5G Communication: current Progress and Future Challenges, Chin. J. Mech. Eng. 2 (2023) 100065, https://doi.org/10.1016/j.cjmeam.2023.100065.

[33] Y.Z.N. Htwe, M. Mariatti, Printed graphene and hybrid conductive inks for flexible, stretchable, and wearable electronics: progress, opportunities, and challenges, J. Sci. 7 (2022) 100435, https://doi.org/10.1016/j.jsamd.2022.100435.

[34] S.L. Merilampi, T. Bjorninen, A. Vuorimaki, L. Ukkonen, P. Ruuskanen, L. Sydanheimo, The effect of conductive ink layer thickness on the functioning of printed UHF RFID antennas, Proc. IEEE 98 (2010) 1610–1619, https://doi.org/10.1109/JPROC.2010.2050570.

[35] I. Ibanez Labiano, D. Arslan, E. Ozden Yenigun, A. Asadi, H. Cebeci, A. Alomainy, Screen Printing Carbon Nanotubes Textiles Antennas for Smart Wearables, Sensors (Basel) 21 (2021), https://doi.org/10.3390/s21144934.

[36] P. Lakkala, S.R. Munnangi, S. Bandari, M. Repka, Additive manufacturing technologies with emphasis on stereolithography 3D printing in pharmaceutical and medical applications: a review, Int. J. Pharmaceutics 5 (2023) 100159, https://doi.org/10.1016/j.ijpx.2023.100159.

[37] M.I. Mohd Ghazali, ADDITIVE MANUFACTURING FOR ELECTRONIC SYSTEMS (AMES), 2019. https://doi.org/10.25335/d4b0-5z28.

[38] M.H. Chowdhury, Q.D. Hossain, M. Azad Hossain, R.C.C. Cheung, Single feed circularly polarized crescent-cut and extended corner square microstrip antennas for wireless biotelemetry, Int. J. Electri. Comput. Eng. 9 (2019) 1902–1909, https://doi.org/10.11591/ijece.v9i3.pp1902-1909.

[39] S.K. Noor, M. Jusoh, T. Sabapathy, A.H. Rambe, H. Vettikalladi, A.M. Albishi, M. Himdi, A Patch Antenna with Enhanced Gain and Bandwidth for Sub-6 GHz and Sub-7 GHz 5G Wireless Applications, Electronics (Switzerland) 12 (2023), https://doi.org/10.3390/electronics12122555.

[40] C.A. Balanis, Antenna Theory Analysis and Design, 2005.

[41] A. Darvishzadeh, K. Nasouri, Manufacturing, modeling, and optimization of nickel-coated carbon fabric for highly efficient EMI shielding, Surf. Coat. Technol. 409 (2021) 126957, https://doi.org/10.1016/j.surfcoat.2021.126957.

[42] C. Sherwin, S. Bhat, S.P. Hebbar, Effects of Current Density on Surface Morphology and Coating Thickness of Nickel Plating on Copper Surface, Turkish J. Comput. Math. Edu. 12 (2021) 79–83. https://turcomat.org/index.php/turkbilmat/article/view/4047.

[43] A. Boukhouiete, S. Boumendjel, N.E.H. Sobhi, Effect of current density on the microstructure and morphology of the electrodeposited nickel coatings, Turk J. Chem. 45 (2021) 1599–1608, https://doi.org/10.3906/kim-2102-46.

[44] N.N. Le, T.C.H. Phan, A.D. Le, T.M.D. Dang, M.C. Dang, Optimization of copper electroplating process applied for microfabrication on flexible polyethylene terephthalate substrate, Adv. Nat. Sci. 6 (2015), https://doi.org/10.1088/2043-6262/6/3/035007.

[45] X. Huang, T. Leng, M. Zhu, X. Zhang, J. Chen, K. Chang, M. Aqeeli, A.K. Geim, K. S. Novoselov, Z. Hu, Highly Flexible and Conductive Printed Graphene for Wireless Wearable Communications Applications, Sci. Rep. 5 (2015) 1–8, https://doi.org/10.1038/srep18298.

[46] Y. Gao, H. Zhang, J. Jiu, S. Nagao, T. Sugahara, K. Suganuma, Fabrication of a flexible copper pattern based on a sub-micro copper paste by a low temperature plasma technique, RSC Adv. 5 (2015) 90202–90208, https://doi.org/10.1039/c5ra18583a.

[47] Y. Kim, B. Lee, S. Yang, I. Byun, I. Jeong, S.M. Cho, Use of copper ink for fabricating conductive electrodes and RFID antenna tags by screen printing, Curr. Appl. Phys. 12 (2012) 473–478, https://doi.org/10.1016/j.cap.2011.08.003.

[48] M. Mieszkowska, M. Grdeń, Electrochemical deposition of nickel targets from aqueous electrolytes for medical radioisotope production in accelerators: a review, J. Solid State Electrochem. 25 (2021) 1699–1725, https://doi.org/10.1007/s10008-021-04950-w.

[49] F. Doğan, M. Uysal, E. Duru, H. Akbulut, S. Aslan, Pulsed electrodeposition of Ni-B/TiN composites: effect of current density on the structure, mechanical, tribological, and corrosion properties, J. Asian Ceramic Soc. 8 (2020) 1271–1284, https://doi.org/10.1080/21870764.2020.1840704.

[50] J.M. Lee, K.K. Jung, J.S. Ko, Formation of nickel microcones by using an electrodeposition solution containing H3BO3, Curr. Appl. Phys. 16 (2016) 261–266, https://doi.org/10.1016/j.cap.2015.12.010.

[51] P. Augustyn, P. Rytlewski, K. Moraczewski, A. Mazurkiewicz, A review on the direct electroplating of polymeric materials, J. Mater. Sci. 56 (2021) 14881–14899, https://doi.org/10.1007/s10853-021-06246-w.

[52] Y. Liu, X. Xu, M. Sadd, O.O. Kapitanova, V.A. Krivchenko, J. Ban, J. Wang, X. Jiao, Z. Song, J. Song, S. Xiong, A. Matic, Insight into the Critical Role of Exchange Current Density on Electrodeposition Behavior of Lithium Metal, Adv. Sci. 8 (2021) 1–11, https://doi.org/10.1002/advs.202003301.

[53] R. Rohini, S. Bose, Electrodeposited carbon fiber and epoxy based sandwich architectures suppress electromagnetic radiation by absorption, Composites Part B 161 (2019) 578–585, https://doi.org/10.1016/j.compositesb.2018.12.123.

[54] H. Li, J. Liu, T. Xu, J. Xia, X. Tan, Z. Tao, Fabrication and optimization of high aspect ratio through-silicon-vias electroplating for 3D inductor, Micromachines (Basel) 9 (2018), https://doi.org/10.3390/mi9100528.

[55] N. Li, P. Li, L. Song, Effect of Surface Roughness in Micro-nano Scale on Slotted Waveguide Arrays in Ku-band, Chin. J. Mech. Eng. (English Edition) 30 (2017) 595–603, https://doi.org/10.1007/s10033-017-0132-2.